PROGRESS IN COLOR, COLORANTS AND COATINGS

available online @ www.pccc.icrc.ac.ir

Progress in Color Colorants Coating 19 (2026), 297-315

Ministry of Science, Research and Technology
Institute for Color Science & Technology

Optimizing Electrophoretic Deposition Parameters and Corrosion Resistance of Nano-Hydroxyapatite/Chitosan Coatings on Ti-6Al-7Nb Alloy Under Various Current Types

Y. Muhi Abdulsahib, A. M. Mustafa*, M. H. Abdulkareem
Department of Metallurgical Engineering, College of Production Engineering and Metallurgy, University of Technology, P.O. Box: 35010, Baghdad, Iraq

ARTICLE INFO

Article history:
Received: 18 Sept 2025
Final Revised: 25 Oct 2025
Accepted: 01 Nov 2026
Available online: 22 Dec 2025

Keywords:
Ti-6Al-7Nb alloy
Electrophoretic deposition (EPD)
Hydroxyapatite (HA)
Corrosion resistance
Simulated body fluid (SBF)

ABSTRACT

Electrophoretic deposition (EPD) is a highly effective technique for modifying biomaterial surfaces, particularly in biomedical applications. This study investigates the influence of current types-direct current (DC), pulsed direct current (PDC), and alternating current (AC)-on EPD parameters, specifically applied voltage and deposition time, for nano-hydroxyapatite/chitosan (HA/CS) coatings on Ti-6Al-7Nb biomedical substrates. Surface morphology and cross-sectional thickness were characterized using optical and scanning electron microscopy, while adhesion tests assessed the bonding strength between the coating and substrate. Electrochemical polarization tests in simulated body fluid (SBF) were performed to evaluate corrosion resistance. For optimization, Taguchi's statistical design of experiments was applied to identify the most significant factors and determine optimal deposition conditions. Results showed that a 16.5 µm-thick HA/CS coating was obtained using PDC at 70 V for 6 minutes with an 800-grit finish. Under these conditions, enhanced adhesion and uniform coating distribution were achieved. Analysis of variance (ANOVA) indicated that applied voltage (70.30 %) and deposition time (80.10 %) were the dominant factors influencing coating thickness and adhesion. Electrochemical evaluation confirmed improved corrosion resistance, with the corrosion rate reduced from 9.662×10^{-3} mm/year for the uncoated alloy to 2.23×10^{-3} mm/year for the coated alloy. Overall, PDC at optimized conditions produced a well-adhered, uniformly distributed HA/CS coating with superior corrosion protection, highlighting the potential of EPD for biomedical implant surface modification. Prog Color Colorants Coat. 19 (2026), 297-315© Institute for Color Science and Technology.

1. Introduction

Nowadays, pure Titanium (Ti) and Ti-based alloys are widely used as metallic biomaterials in the orthopedic and dental fields due to their unique mechanical properties, particularly their low modulus of elasticity and impressive strength-to-weight ratio, along with their biocompatibility, low toxicity, and outstanding corrosion resistance [1-5]. Ti-6Al-4V and Ti-6Al-7Nb alloys are common Titanium alloys used in implant biomaterial applications compared to CP-Ti because their mechanical strength is superior to that of CP-Ti, and they exhibit high resistance to corrosion and wear. However, vanadium (V) is cytotoxic, and if Vions are released from the Ti-6Al-4V alloy withinthe human body, they can lead to several complications, such as Alzheimer's [6-8]. Therefore, new titanium alloys with non-toxic elements such as Nb, Zr, Ta, Mo, and Fe have been developed to overcome these issues [7, 9, 10].

*Corresponding author: * Ali.M.Mustafa@uotechnology.edu.iq
https://doi.org/10.30509/pccc.2025.167666.1451

Among these alloys, the Ti-6Al-7Nb alloy is a new-generation implant material developed by replacing the controversial element in Ti6AL4V with niobium, which is considered a nontoxic material in its interaction with human tissue [7, 10-12]. The Ti-6Al-4V alloy, which has been used for many years in medical applications, can potentially be replaced by the Ti-6Al-7Nb alloy, which is approved for clinical use [6, 7]. From a biochemical perspective, titanium alloys are considered nearly inert materials because they do not chemically or biologically bond with tissues when implanted within the human body [6, 13]. To enhance the bioactivity and anti-corrosion properties of titanium alloys, surface modification with bioactive inorganic materials, such as hydroxyapatite (HA) or bioactive glasses, is a common method [1, 12, 14]. It is well known that HA chemical formula [Ca_{10} $(PO_4)_6(OH)_2$] coatings have been used for several years because they enhance the bioactivity of the implant surface; they possess structural, chemical, and biological characteristics similar to those of human bone, which promotes osseointegrationand non-toxicity [2, 6, 15-17].

Hydroxyapatite is characterized by its ideal bio-compatibility, since the nanoparticles in nano HA coatings resemble the inorganic molecules found in human bone, which results in adequate connection with living bone tissue [9, 18, 19]. Coatings by HA reduce the release of metallic ions by providing a barrier to the metallic implant materials [12]. The adhesion of the coating to the substrate is a crucial factor that influences the long-term stability of the implants.Some studies have indicated that the bonding between interfaces can be improved by adding polymers, such as chitosan (CS), collagen, gelatin, and polylactide, to the coatings [15]. Since CS is a nontoxic biopolymer with strong hydrophilic and antibacterial properties, it is frequently used in biomedical materials. The electrostatic contact is what gives CS its antibacterial properties. Chitosan exhibits strong antibacterial properties due to its positively charged amino groups interacting with the negatively charged microbial cell membranes, resulting in the leakage of bacterial internal components [15, 20]. Recently, HA/ CS composites have often been used as scaffolds, dressings, and coatings for implants.

Electrophoretic deposition (EPD) is one of the most promising techniques for depositing nanocomposite HA/CS coatings or bioactive glass coatings on metal surfaces, because of its simplicity and low cost, and it can be performed at room temperature [6, 18, 21-24]. Additionally, it leads to uniform coatings that can be applied to any complex shapes [18, 22, 23]. Thecoating quality results from coating operations via the EPD technique are affected by several factors,such as deposition period, the applied voltage, and the suspension concentration [12, 22, 23]**.**

In previous studies, however, the comparison of these factors was not thoroughly examined to identify the optimal conditions for producing a coating layer with suitable characteristics. Therefore, this work aims to optimize the EPD variables, including voltage and time, as well as grinding degree (surface roughness), by using different current types (DC, AC, and PDC). The study employs the Taguchi method, focusing on the thickness and adhesion of the nano-HA/CS coating on the Ti-6Al-7Nb alloy, which influence the bonding between the substrate and the coating. Corrosion behavior and SEM analysis are considered for the optimal condition. Both adhesion and corrosion resistance characteristics play a crucial role in biomedical applications, particularly in bone replacement applications.

2. Experimental

2.1. Material

The material used as substrate in this researchis a Ti6Al7Nb alloy, commonly used as an implant in biomedical applications. The rod of Ti6Al7Nb alloy with dimensions of 20mm in diameter and 50 mm in length was received from Baoji Jinsheng Metal Materials Co., Ltd. The X-ray energy-dispersive spectrometer (EDS) in Figure 1 shows that Ti6Al7Nb (Standard) alloy is primarily composed of Titanium (Ti), with Aluminum (Al) and Niobium (Nb) as key alloy ingelements. Specifically, it contains 5.5-6.5 % Aluminum, 6.5-7.5 % Niobium, and the balance is Titanium.

Additionally, it contains trace amounts of other elements like Tantalum (Ta), Iron (Fe), Oxygen (O), Carbon (C), and Nitrogen (N), but these are typically present in very smallpercentages, often below 0.5 %. The chemical composition of the Ti_6Al_7Nb alloy is shown in Table 1.

Table 1: Chemical composition of the Ti6Al7Nb alloy.

Element	Atomic %	Atomic % Error	Weight %	Weight % Error
Al	5.8	0.1	5.9	0.0
Ti	87.3	0.2	87.3	0.3
Nb	6.9	0.2	6.8	0.4

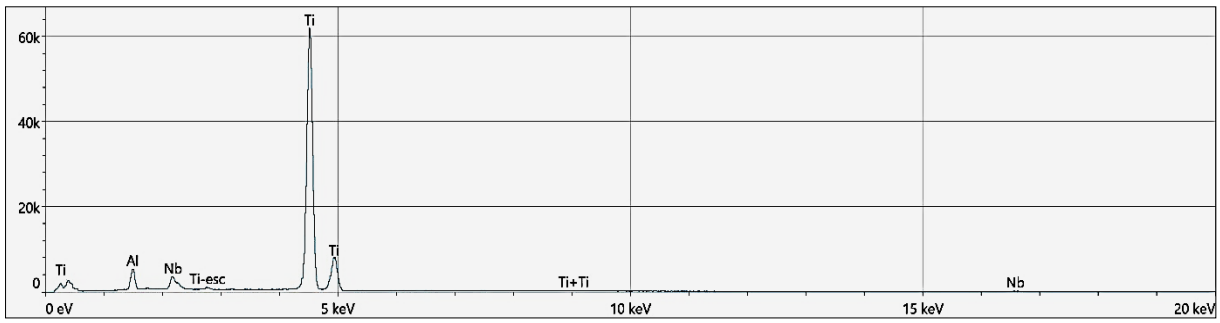

Figure 1: EDS of the Ti6Al7Nb alloy.

The Ti_6Al_7Nb rod substrate was cut into a half-circle sample with a 10 mm radius and 2 mm thickness using a wire-cutting machine at a moderate cutting speed 2 mm/min to prevent heating during the process, as shown in Figure 2. Then, the samples' surfaces were ground using a manual grinder (Struers - Labopol 5 model) with silicon carbide (SiC) emery paper and washed with water to obtain a final surface roughness. The number of samples was set to be 9 according to Taguchi's approach and separated into 3 groups, each consisting of 3 samples. They were ground to three degrees of grinding (surface roughness): 220, 500, and 800 grit for the first, second, and third groups, respectively. Then, the samples were cleaned in an ultrasonic cleaner (UNISOINCS - FX p 12 model) using ethanol and distilled water for 30 minutes, respectively. Finally, the samples were dried in a dryer at 25 °C.

2.2. Suspension coating preparation

A Hydroxyapatite powder (60 nm, molar mass 502.31, purity of 96 %) from Sigma Aldrich, chitosan powder (60 nm, with purity > 99 %) from Sigma Aldrich, acetic acid, distilled water, and absolute ethanol (density = 0.79 g/cm^3) were used to prepare a suspension solution for electrophoretic deposition (EPD). Firstly, 100 mL of suspension solution is prepared by dissolving 0.05 g/ 100 mL of chitosan using 1 % acetic acid in a glass beaker [25-28]. Secondly, absolute ethanol (99.96 purity) and 5 % of distilled water were added to the glass beaker. The mixture was magnetically stirred for 15 minutes, and then 0.3 g/100 mL nano HA powder material was added to the glass beaker. After that, the suspension was covered with parafilm to prevent evaporation. All suspensions were deagglomerated for 24 hours using a magnetically stirred (model LMS-1003) to ensure homogenization. Finally, a high-energy sonicator (Ultrasonic Processor, UNISONICS PYT Ltd, type FXp12) was used for 30 minto break up fragile agglomerates and to homogenize the dispersion of particles in the suspension. A pH meter was used to adjust the pH value of solutions to 4 by using a pH meter.

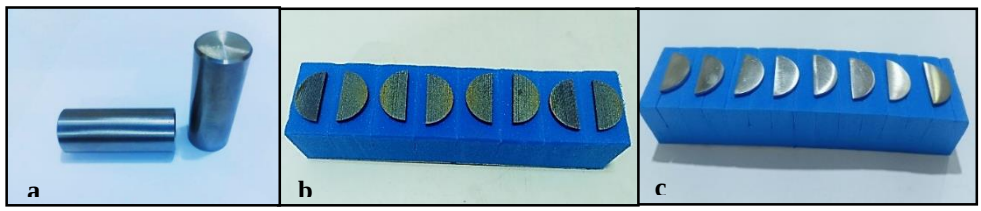

Figure 2: a) Ti6Al7Nb alloy rod as received, b and c) samples before and after grinding.

2.3. Electrophoretic deposition

The electrophoretic deposition (EPD) was carried out using a locally made multi-mode power supply in a standard two-electrode system. The titanium alloy substrate, measuring 10 mm radius and 2 mm thickness, served as the cathode, whereas the 316L stainless steel, with dimensions of 10 mm by 20 mm by 2 mm, functioned as the anode. Stainless steel is stable in suspension, conductive, and widely used as a counter electrode in EPD due to its corrosion resistance and availability. The distance between the electrodes was fixed to be 10 mm. The design for the EPD system employed in this work is shown in Figure 3 [23]. The EPD cell consists of a beaker with two electrodes immersed in the suspension. During the deposition process, various parameters were used, including current typespulse direct current(PDC), direct current (DC), and alternating current (AC), applied voltages of 30, 50, and 70 volts, and deposition times of 2, 4, and 6 minutes. Subsequently, the samples' coating was dried by air at ambient temperature.

3. Design of experiment

In this study, Taguchi's method was employed to identify the optimal design parameters that improve performance and reduce the costs associated with the design. It is based on MATLAB programming as a statistical tool for designing experiments (DOE). The input parameters are referred to as factors, and the outputs are referred to as response variables. This method was employed to analyze data and estimate the effects of various EPD process parameters or factors on the output. It allowed systematic optimization of deposition parameters (voltage, current type, time, surface finish) with fewer experiments, identifying the most influential factors on coating thickness and adhesion. The HA layer was deposited experimentally using an L9 [33] orthogonal array. Table 2 presents the experiment design based on Taguchi's method.

Table 2: L9 Orthogonal Array of variables and the corresponding levels of Nano HA/CS coating.

Sample No.	Current Type	Voltage (V)	Time (min)	Grinding Degree (grit)
1	1	1	1	1
2	1	2	2	2
3	1	3	3	3
4	2	1	2	3
5	2	2	3	1
6	2	3	1	2
7	3	1	3	2
8	3	2	1	3
9	3	3	2	1

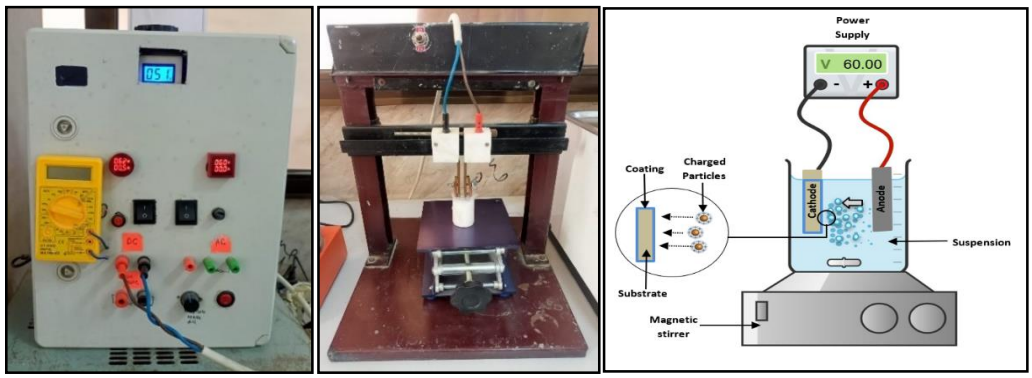

Figure 3: EPD coating cell [23].

4. Coating characterization method

4.1. Suspension stability measurement

To confirm the stability of the coating suspension, the zeta potential was measured. Zeta potential (Zeta Plus Model) was used to assess the stability of the suspension particles. It's an essential test in EPD to ensure the acquisition of a homogeneous solution suspension that leads to a homogeneous coating layer.

4.2. Microstructure evaluation

An optical microscope (OPTIKA 4083 B5 model) connected to a camera was used to measure the coating thickness and topography of coating samples. A scanning electron microscope (SEM), TESCAN Model-20,000 kV, was used to determine the surface morphology of the optimum sample. Before the investigation, an Au film was applied onto the coating surfaces to reduce the charging effect and enhance the signal-to-noise ratio.

4.3. Adhesion evaluation

To determine the quality of the coating layer, a tap test was performed to measure the bond strength between the coating layer and the substrate. Tape test (Cross-cut test)involves cutting a grid pattern into the coating and then applying tape to visually assess the adhesion. It was according to the ASTM "D 3359-B" standard.

4.4. X-ray diffraction analysis

X-ray diffraction (XRD) has been used to analyze and determine the existing phases of the Ti-6Al-7Nb alloy substrate, HA nano powder, and the best coated sample, using a (X2500 model)with CuK radiation (λ = 1.5405 Å) and a scan speed of (10 deg/min) at a voltage (30,000 kV) and a current (20 mA).

4.5. Biocorrosion measurement

Electrochemical corrosion testing was conducted on uncoated and coated samples in a simulated body fluid (SBF) at 37 °C, using a saturated calomel electrode (SCE) as the reference electrode. The composition of the SBF solution used in the biocorrosion test is illustrated in Table 3 [1, 24]. The exact pH value of the solution is 7.1-7.3. The area of the coated surface exposed to the corrosion was 0.385 cm^2. Both edges and other sides of the electrode were masked with lacquer and were dried in air. The sample and SCE electrodes were dipped into the electrolyte solution (SBF) to study the corrosion process. The polarization and open circuit potential (OCP) measurements were performed on uncoated and coated titanium substrate samples. Critical parameters, including corrosion potential (E_{corr}), corrosion current (I_{corr}), andanodic (β_a) and cathodic (β_c) Tafel slopes, were evaluated from the polarization curves. Electro-chemical experiments were performed using a model (CHI 604e) with the aid of commercial software (Corr. lab). Samples were immersed in SBF, and OCP was monitored for 20 min. Polarization scans were per-formed at a scan rate of 0.01 V/s, ranging from -0.12 V to 3.0 V compared to the Saturated Calomel Electrode (SCE). The corrosion rate of the coated and uncoated sampleswascalculated according to ASTM G102.

5. Results and Discussion

5.1. Stability of HA/CS Suspension

The stability of the suspension and the uniformity of the resulting coating were critically evaluated through zeta potential measurements, which are essential indicators of colloidal stability in electrophoretic deposition (EPD) processes. Zeta potential reflects the magnitude of the electrostatic repulsion or attraction between particles in a suspension, and higher absolute values (typically > ±30 mV) are associated with greater dispersion stability, preventing agglomeration.

Table 3: Chemical composition of simulated body fluid (SBF).

Reagents	NaCl	$NaHCO_3$	KCl	$K_2HPO_4{\cdot}3H_2O$	$MgCl_2{\cdot}2H_2O$
C (g/L)	7.996	0.350	0.224	0.228	0.305
Reagents	$CaCl_2$	Na_2SO_4	$(CH_2OH)_3CNH_2$	1 M HCl	-
C (g/L)	0.278	0.071	6.057	40	-

In this study, the nano-HA/CS suspension exhibited a positive zeta potential of 23 mV, as illustrated in Figure 4. This positive charge indicates that the suspension is sufficiently stable and that the nanoparticles will migrate toward the cathode during deposition, confirming cathodic deposition behavior. It shows moderate stability, preventing severe agglomeration, ensuring uniform particle migration and deposition.

The presence of HA in the chitosan matrix appears to significantly improve the electrokinetic behavior of the suspension. Specifically, the HA nanoparticles likely enhance the dispersion and surface charge of the chitosan molecules, leading to an increase in the overall zeta potential compared to chitosan-only suspensions. This is consistent with prior findings [29, 30] which demonstrated that HA particles contribute to stabilizing the biopolymer network and reducing the tendency of particle agglomeration. As a result, the improved zeta potential translates into a more homogeneous and uniform coating layer, which is crucial for ensuring consistent surface coverage and functional performance in biomedical applications.

5.2. Microstructure results

The cross-sectional morphology and thickness of the HA/CS coating samples were thoroughly examined using an optical microscope with a magnification power of 100X to assess the uniformity, continuity, and structural integrity of the deposited layers. The visual results obtained from this microscopic analysis are presented in Figure 5. Among the evaluated samples, the coating produced under pulsed direct current (PDC) conditions exhibited the most favorable characteristics. Specifically, when an applied voltage of 70 V was used with a deposition time of 6 minutes and a substrate surface roughness prepared using 800-grit, the resulting HA/CS coating achieved the highest recorded thickness of 16.5µm. This coating appeared homogenous, dense, and continuous, indicating excellent deposition quality and surface coverage. Pulsed current reduces bubble formation, promotes uniform deposition, and finer grinding increases surface contact, resulting in denser coatings.

In contrast, the sample coated under direct current (DC) mode, particularly sample number 5, which was processed using a lower applied voltage of 50 V, the same deposition time of 6 minutes, and a rougher surface preparation using 220-grit SiC paper, demonstrated a reduced coating thickness of 14.05 µm. Despite this thinner coating, it exhibited a relatively low coating removal area rate, implying strong adhesion between the coating and the titanium substrate. This suggests that even with reduced thickness, the coating quality remained adequate due to good interfacial bonding.On the other hand, coatings produced under alternating current (AC) conditions displayed inferior performance in terms of both coating thickness and adhesion. The thickness of the coating layers formed under AC parameters was noticeably lower compared to those formed under PDC and DC conditions, and the material removal area was significantly higher, indicating weaker adhesion and a less effective deposition process.

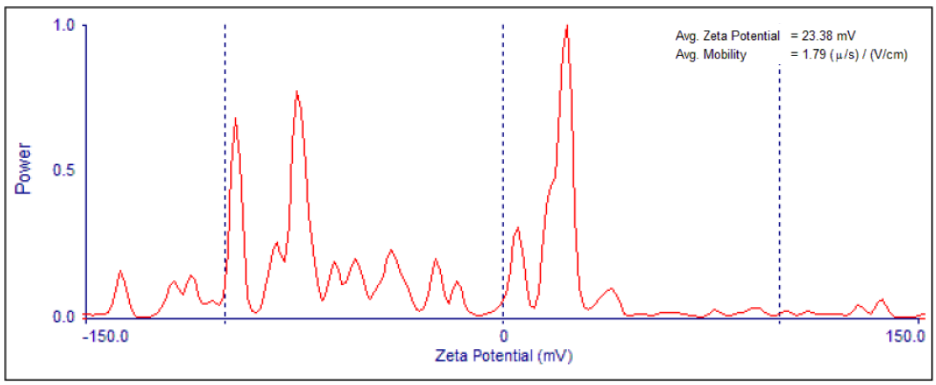

Figure 4: Zeta potential of HA/CS suspension coating.

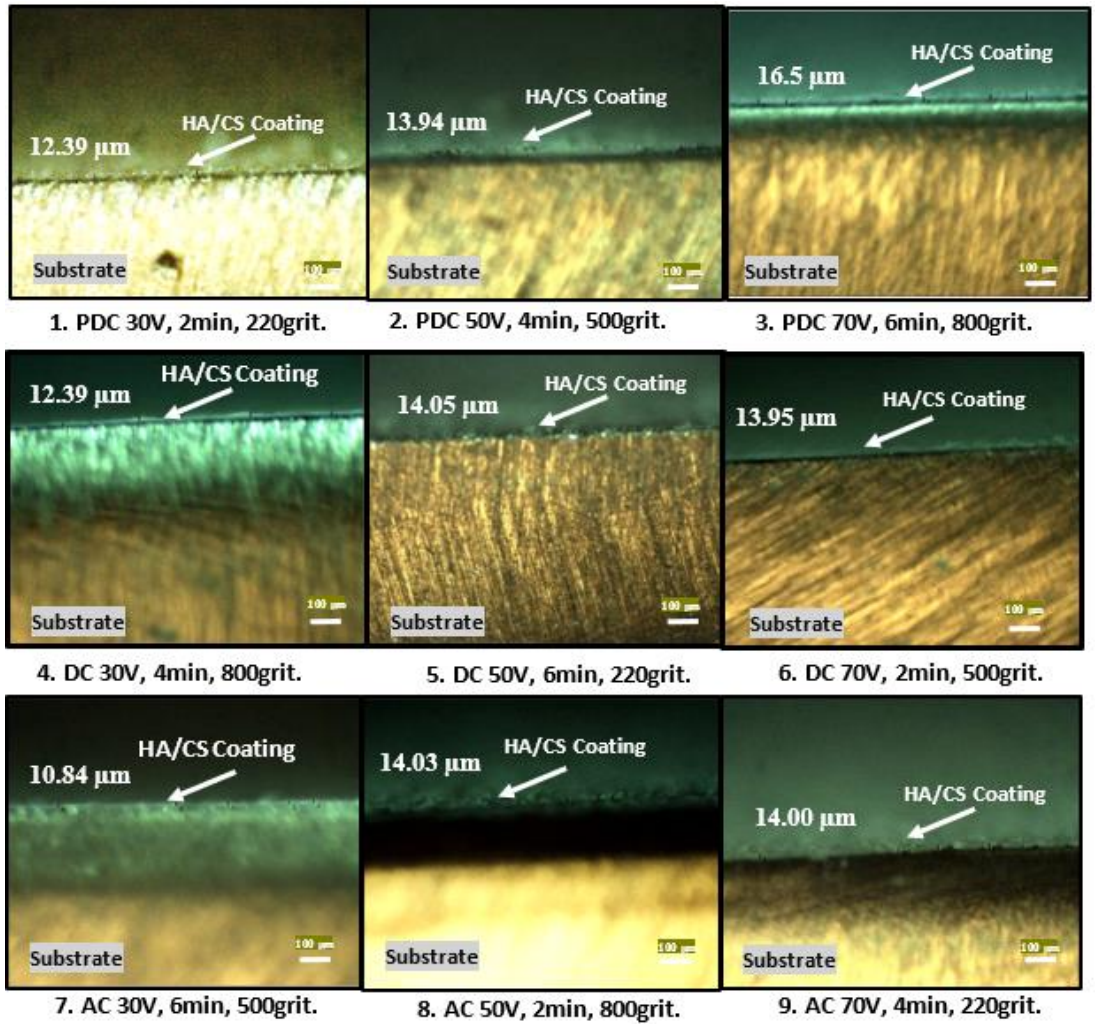

Figure 5: Cross-section of HA/CS coating layer.

The surface topography of the coated samples was carefully analyzed using an optical microscope to evaluate the quality and uniformity of the applied HA and chitosan CS layers. The visual examination results are presented in Figure 6, which illustrates the morphological characteristics of the coating layers formed under various deposition conditions. Notably, a uniform and homogeneous HA coating layer was observed on samples 3, 5, and 9. These coatings were produced under specific parameter combinations as follows: sample 3 was prepared under pulsed direct current (PDC) conditions at an applied voltage of 70 V for a deposition time of 6 minutes using a substrate pre-treated with 800-grit degree of grinding; sample 5 was coated under direct current (DC) conditions at 50 V for 6 minutes on a 220-grit surface; and sample 9 was deposited under alternating current (AC) conditions at 70 V for 4 minutes using a 220-grit surface. The coatings on these samples appeared smooth and continuous, with no visible cracks or delamination, indicating a good degree of adhesion and surface coverage. Additionally, the incorporation of chitosan in the HA/CS composite coatings contributed to moderately hydrophilic surface characteristics. This behavior is attributed to the hydrophilic nature of chitosan, which enhances the surface energy and potentially improves the interaction between the coating and biological environments.

Figure 7a and b show the SEM for coating thickness and topography of the sample under condition PDC, 70 V applied voltage, and 6 min deposition time. A coating thickness of HA/CS can be illustrated in Figure 7a. Figure 7b shows the topography of the HA/CS coating.

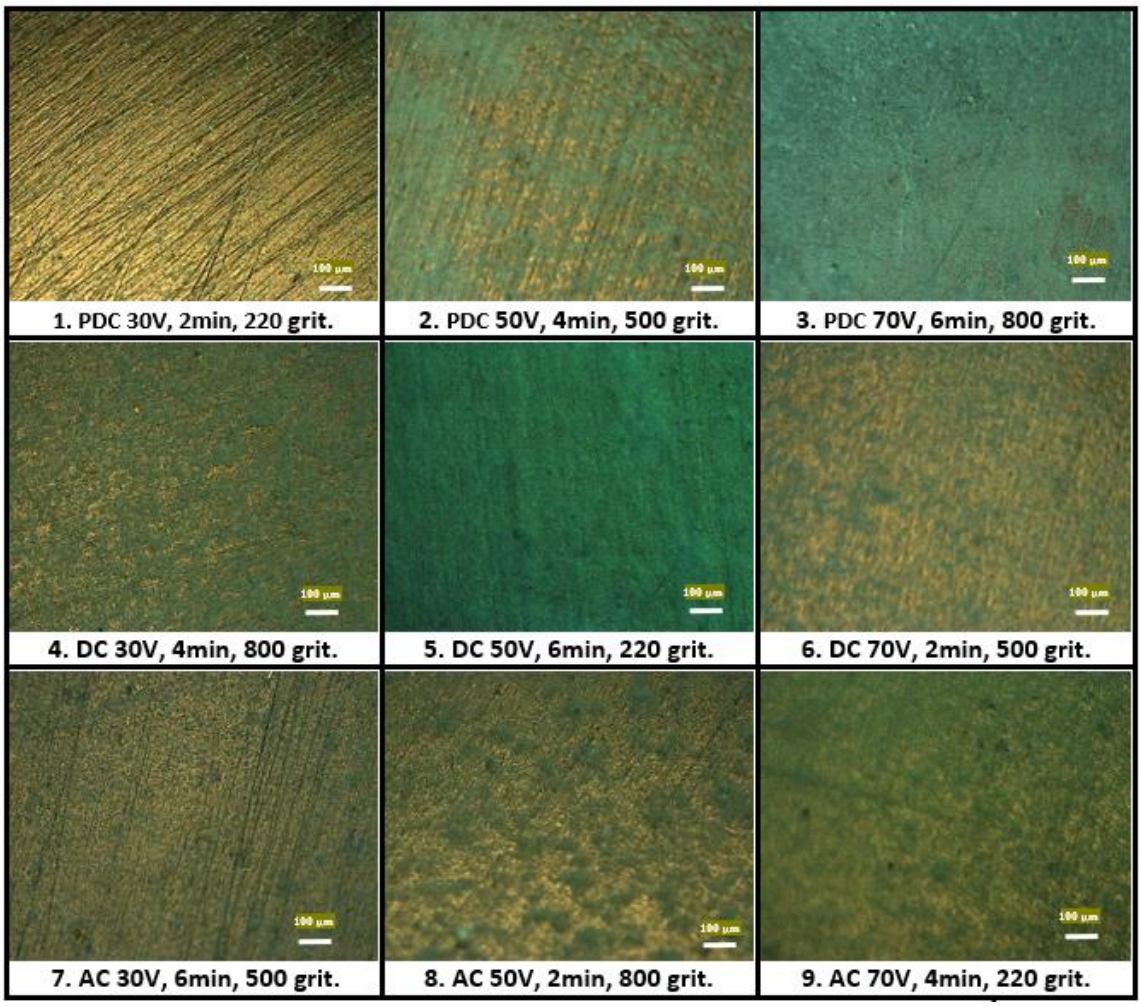

Figure 6: Surface topography of the HA/CS coating on the Ti_6Al_7Nb.

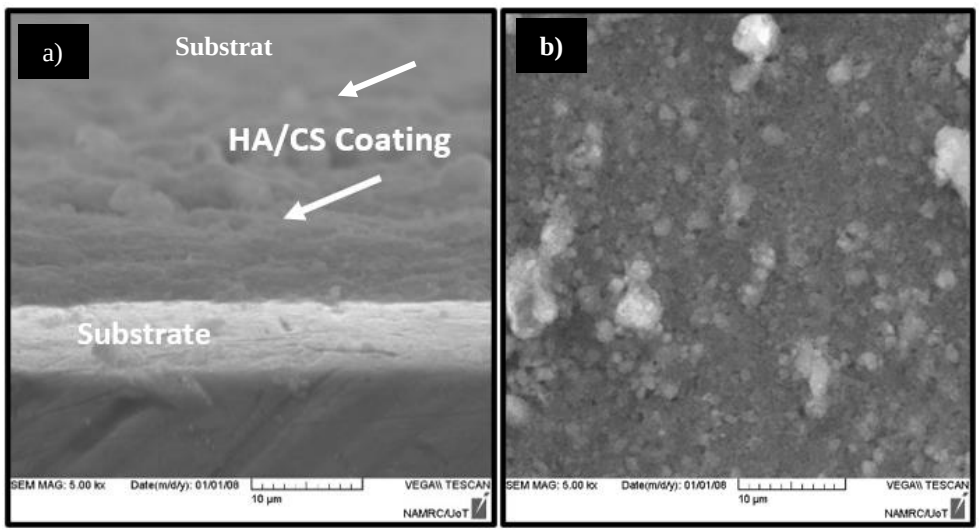

Figure 7: SEM of the a) cross-section coating layer for sample 3 and b) a topography of the HA/CS coating layer.

5.3. Adhesion results

Figure 8 presents the adhesion test results using the cross-cut tape method. Among all samples, samples 3, 5, and 4 showed the lowest coating removal area rates, 3.857, 5.048, and 6.258 %, respectively, indicating superior adhesion of the HA/CS coating to the Ti-6Al-7Nb substrate.

Sample 3 with deposited parameters using PDC at 70 V for 6 minutes andan800-gritgrinding degree demonstrated the best adhesion, due to uniform deposition and chitosan's binding effect that reduced internal stresses, attributed to uniform deposition and the binding effect of chitosan. The pulsed current mode enhanced bonding by reducing gas bubble entrapment and internal stresses during the coating formation process.

Sample 5 with deposited parameters using DC at 50 V for 6 minutes and a 220-gritgrinding degree also showed strong adhesion, likely due to its coarse surface finish (220 grit) and sufficient deposition time. Sample 4 with deposited parameters using DC at 30 V for 4 minutes and an 800-gritgrinding degree exhibited moderate performance under lower voltage. In contrast, coatings produced under AC had weaker adhesion, likely due to instability in particle migration caused by continuous polarity reversal. Overall, the results confirm that PDC offers more favorable conditions for achieving strong, stable coatings. The choice of current type significantly affects coating morphology, quality, and process efficiency in electrophoretic deposition. While DC is simple and widely used, PDC provides better control and coating properties. AC may be suitable for

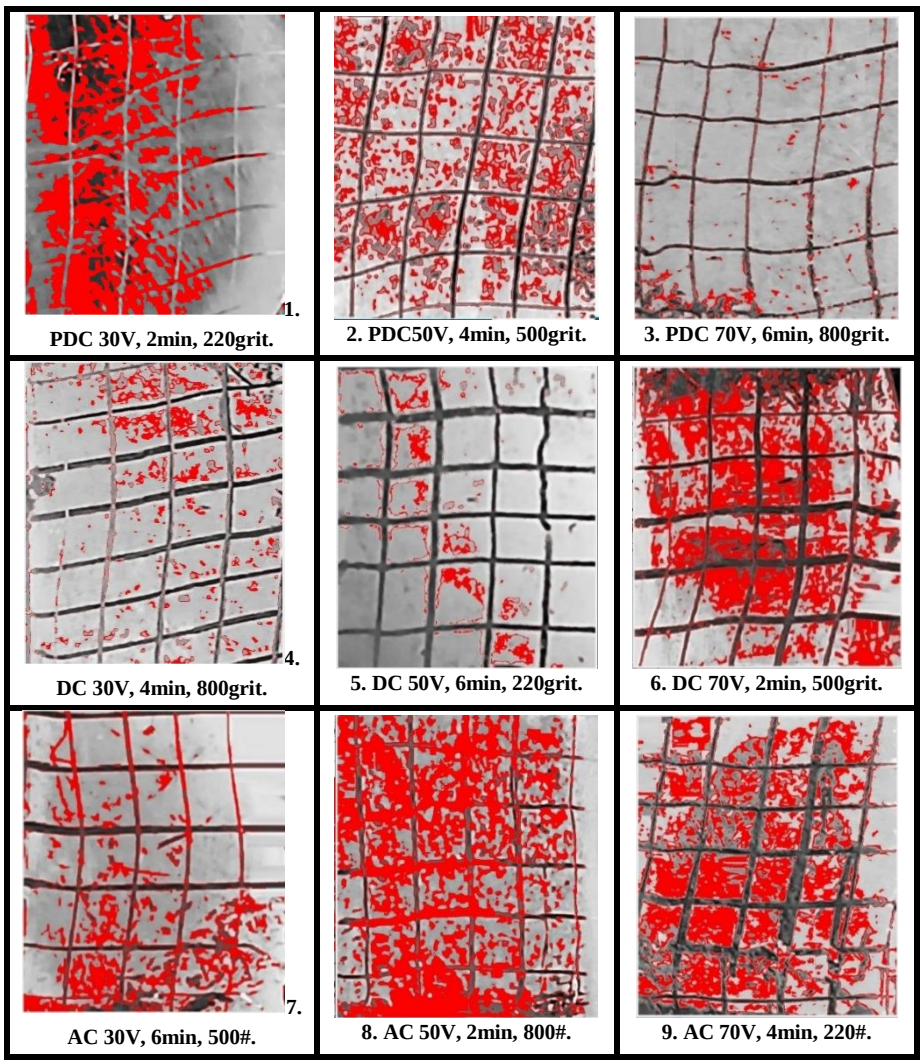

Figure 8: Optical images for the coating's removal area of the HA/CS layer.

specialized applications, but it requires optimized parameters due to its lower net deposition efficiency. As a result, PDC provides the optimal condition because the PDC's on-off cycles create pauses between pulses, allowing relaxation and redistribution of ions. That leads to reduced concen-tration polarization and gas evolution, which enhances the uniformity of the coating.

5.4. Optimization of HA/CS layer deposition

After completing the coating of all the samples by using the EPD cell, the Taguchi statistical approach was employed to determine the optimum conditions for the nano HA/CS coating layer on the Ti-6Al-7Nb substrate. It aims to achieve the highest thickness of the coating layer and the lowest value of the coating removal area rate of material for strong adhesion between the coating layer and the Ti alloy substrate.

5.4.1. Optimization condition for thickness coating

The best optimization was obtained from the signal-to-noise ratio (S/N) for the main effect for the best thickness coating. Table 4 shows the Taguchi approach parameters for coating HA/CS layers deposition on the Ti alloy substrate. Furthermore, the hypothesis of the SNs ratio (where maximum = better) indicates that the experiment has a maximum value of the SNs ratio. The optimum parameters were selected from the S/N as the best one, which was obtained according to the Taguchi design (L9) for the thickness measurement results of HA/CS layers, as shown in Table 5. An optimal coating layer of HA/CS was induced, and the increased thickness of 16.5 μmand S/Ns ratio of 24.3497 were achieved in experiment 3. By considering the SNs ratio, the optimal parameters were identified as the current type is PDC, applied voltage 70 V, deposited time 6 minutes, and800grit, as shown in Figure 9. Experi-mental investigations were carried out under these specific circumstances to determine the thickness, which was found to be 16.5 μm, adequate for obtaining dependable HA/CS thicknesses. As demonstrated in Tables 6 and 7, the primary factors influencing the deposition of the HA/CS layer are voltage (70.30 %), grinding degree (15 %), current type (13.48 %), and duration time (1.22 %).

5.4.2. Optimization condition for adhesion coating

The best optimization was obtained from the signal-to-noise ratio (S/N) for the main effect of the low coating removal area percentage (better adhesion). Furthermore, the hypothesis of the SNs ratio (where the smallest = better) indicates that the experiment has a maximum value of the SNs ratio. The optimum parameters were selected from the S/N as the best one, which was obtained according to the Taguchi design (L9) for the coating removal area measurement results of the HA/CS layer, as shown in Table 9. An optimal coating layer of HA/CS was induced, and the decreased coating removal of 3.857 %, and the S/Ns ratio of (-11.7250) were achieved in experiment 3.

Table 4: Taguchi approach parameters for HA/CS layers deposition.

Sample No.	Current Type	Voltage (V)	Time (min)	Grinding Degree (grit)
1	PDC	30	2	220
2	PDC	50	4	500
3	PDC	70	6	800
4	DC	30	4	800
5	DC	50	6	220
6	DC	70	2	500
7	AC	30	6	500
8	AC	50	2	800
9	AC	70	4	220

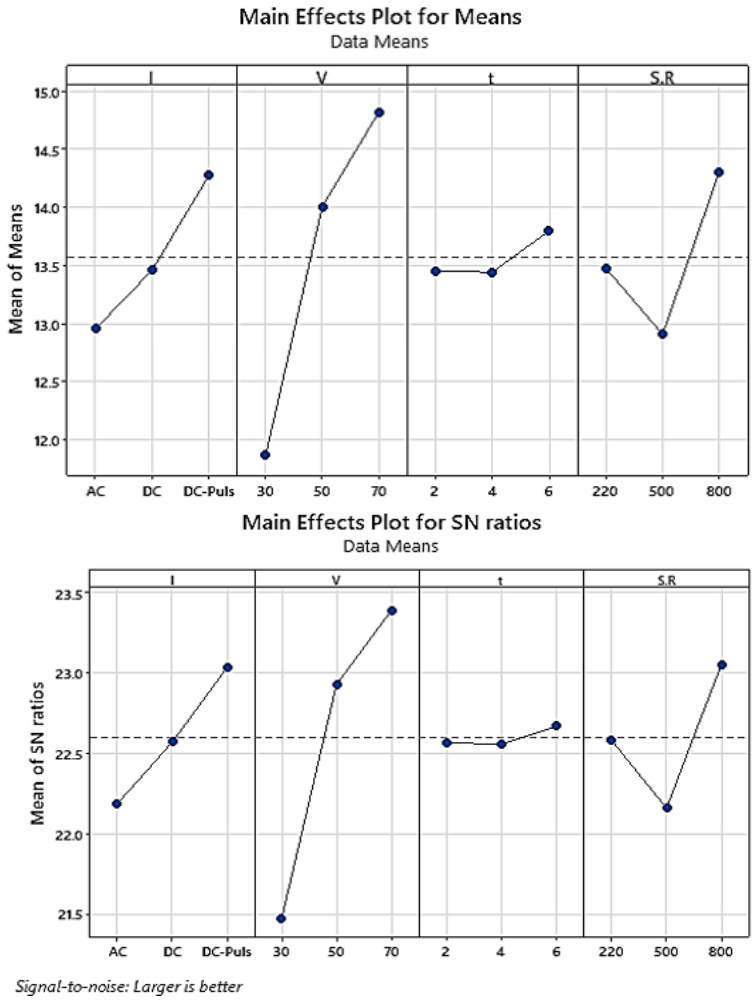

Figure 9: SN ratios and the main effect ofthe coating thickness.

Table 5: Ratio of signal to noise of Taguchi design of (L9) for HA/CS thickness coating layer.

NO.	Current Type	Voltage (V)	Time (min)	Grinding Degree (grit)	Average Thickness (µm)	SNRA1	MEAN1
1	PDC	30	2	220	12.39	21.8614	12.39
2	PDC	50	4	500	13.94	22.8853	13.94
3	PDC	70	6	800	16.5	24.3497	16.50
4	DC	30	4	800	12.39	21.8614	12.39
5	DC	50	6	220	14.05	22.9535	14.05
6	DC	70	2	500	13.95	22.8915	13.95
7	AC	30	6	500	10.84	20.7006	10.84
8	AC	50	2	800	14.03	22.9412	14.03
9	AC	70	4	220	14.00	22.9226	14.00

Table 6: Rank of adjusting thickness-controlling parameters in the HA/CS layer.

Level	I	V	t	G.D.
1	23.66	22.90	24.11	23.58
2	23.89	24.54	24.49	23.63
3	25.70	25.81	24.64	26.04
Delta	2.04	2.91	0.53	2.46
Rank	3	1	4	2

Table 7: Statistical analysis (ANOVA) of HA/CS layer thicknesses.

Variable	DF	Sum of squares SS	Adj MS	R-Sq
I	2	2.6606	1.3303	13.48
V	2	13.8704	6.9352	70.30
t	2	0.2406	0.1203	1.22
S. R	2	2.9590	1.4795	15.00
Errors	0	*	*	*
Total	8	19.7306		100.00

By considering the SN ratio, the optimal parameters were identified as the current type is PDC, 70 V, 6 minutes, and S.R.800 grit, as shown in Figure 10. Experimental investigations were carried out under these specific circumstances to ascertain the coating removal area, which was found to be 3.857 %, which is adequate for obtaining dependable HA/CS adhesion. As demonstrated in Tables 10 and 11, the primary factors influencing the deposition of the HA/CS layer are the duration time 80.10 %, grinding degree 12.64 %, followed by current type6.99 %, and Voltage 0.27 % [12].

Table 9: Ratio of signal to noise of Taguchi design of (L9) for HA/CS adhesion coating layer.

NO.	Current Type	Voltage (V)	Time (min)	Grinding Degree (grit)	CoatingRemove Area	SNRA1	MEAN1
1	PDC	30	2	220	43.050	-32.6795	43.050
2	PDC	50	4	500	28.560	-29.1152	28.560
3	PDC	70	6	800	3.857	-11.7250	3.857
4	DC	30	4	800	6.258	-15.9287	6.258
5	DC	50	6	220	5.048	-14.0624	5.048
6	DC	70	2	500	42.790	-32.6268	42.790
7	AC	30	6	500	18.283	-25.2409	18.283
8	AC	50	2	800	39.772	-31.9915	39.772
9	AC	70	4	220	24.519	-27.7901	24.519

Table 10: Rank of adjusting adhesion s-controlling parameters in the HA/CS layer.

Level	I	V	t	G.D.
1	-28.34	-24.62	-32.43	-24.84
2	-20.87	-25.06	-24.28	-28.99
3	-24.51	-24.05	-17.01	-19.88
Delta	7.47	1.01	15.42	9.11
Rank	3	4	1	2

Table11: Statistical analysis (ANOVA) of HA/CS adhesion layer.

Variable	DF	Sum of squares SS	Adj MS	R-Sq
I	2	146.47	73.235	6.99
V	2	5.69	2.844	0.27
t	2	1679.25	839.623	80.10
S. R	2	265.10	132.552	12.64
Errors	0	*	*	*
Total	8	2096.51	*	100.00

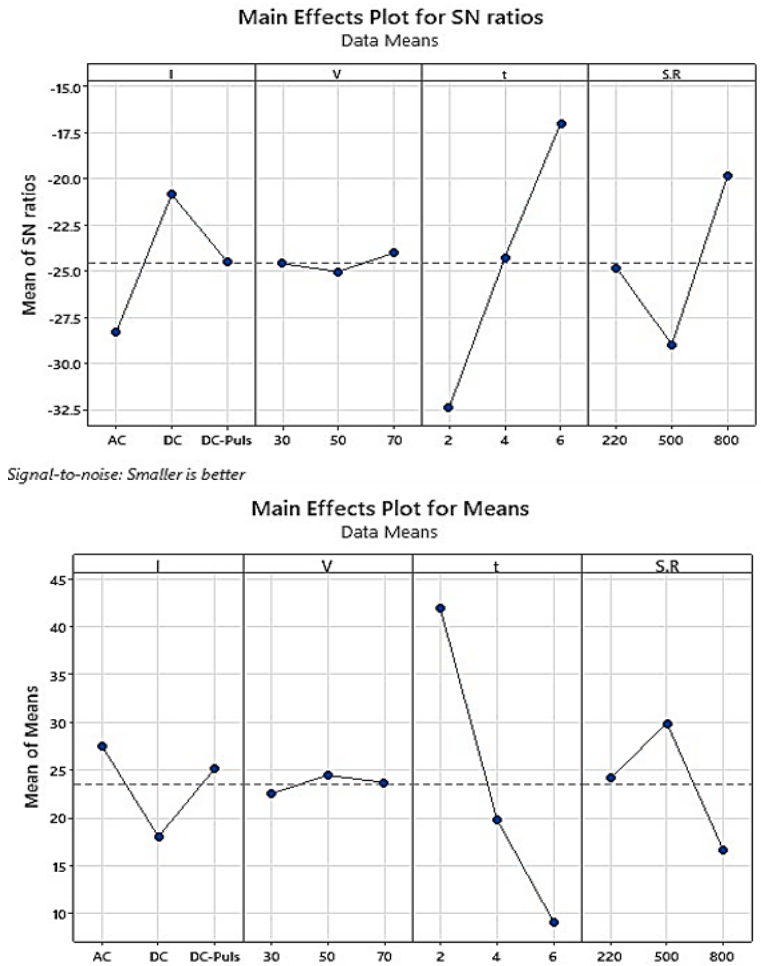

Figure 10: SN ratios and the main effect of adhesion.

5.5. X-Ray diffraction analysis

Figure 11 presents the X-ray diffraction (XRD) pattern of the as-received Ti-6Al-7Nb alloy. The diffraction peaks correspond to a biphasic microstructure composed of both α and β phases, which is consistent with the α+β titanium alloy class. The α phase is a hexagonal close-packed (HCP) structure, primarily stabilized by aluminum (Al), which substitutes into the titanium lattice and enhances its thermal stability. In contrast, the β phase, which adopts a body-centered cubic (BCC) structure, is stabilized by niobium (Nb), a β-stabilizing element that improves corrosion resistance and reduces elastic modulus. The observed diffraction peaks match standard reference data for α-Ti (e.g., (100), (002), (101)) and β-Ti (e.g., (102), (110), and (112)), confirming the dual-phase structure [4, 31, 32]. No secondary phases or intermetallic compounds were detected, indicating the homogeneity and purity of the as-received alloy.

Figure 12 shows the XRD pattern of the HA Nano powder used for the coating process. The diffraction peaks are sharp and clear, indicating high crystallinity of the HA particles. Characteristic peaks for the crystal planes (002), (211), (300), (202), (310), (222), (213), and (004) were observed, matching the standard JCPDS card No. 09-0432 for pure stoichiometric HA [1, 33, 34]. The most intense peak appears at 2θ ≈ 32.4°, which corresponds to the (211) plane, a key peak for hydroxyapatite. This confirms the successful synthesis and phase purity of the HA powder, essential for ensuring bioactivity and osseointegration when used as an implant coating. No secondary calcium phosphate phases such as β-TCP or amorphous phases were detected, further supporting the phase purity and stability of the HA nanoparticles used in this study.

The XRD pattern of the best-coated sample (No. 3) is illustrated in Figure 13. Most of the dominant peaks for HA appear between 25°-35° and 40°-55°. The most intense peak is at ~32.4°, corresponding to the (211) plane of HA. Other peaks include 34°, 39°, 48°, 50°, and 65° confirming the formation of crystalline HA [12, 35]. Peaks of Ti alloy are visible around 36°, 39.2°, 41.5°, 54°, 64.5°, 71.5°, and 75°. These characteristics are typical of titanium and arise because the X-ray penetrates the thin HA coating, allowing it to detect the metallic substrate. The prominent HA peaks indicate excellent crystallinity and phase purity, whereas the peaks from Ti, Al, and Nb suggest a contribution from the substrate owing to the relatively thin coating. The lack of decomposition phases (TCP, CaO) serves as a favorable sign of coating stability, indicating its suitability for biomedical applications.The presence of crystalline HA peaks with no decomposition phases, confirming stable, phase-pure coatings suitable for biomedical use.

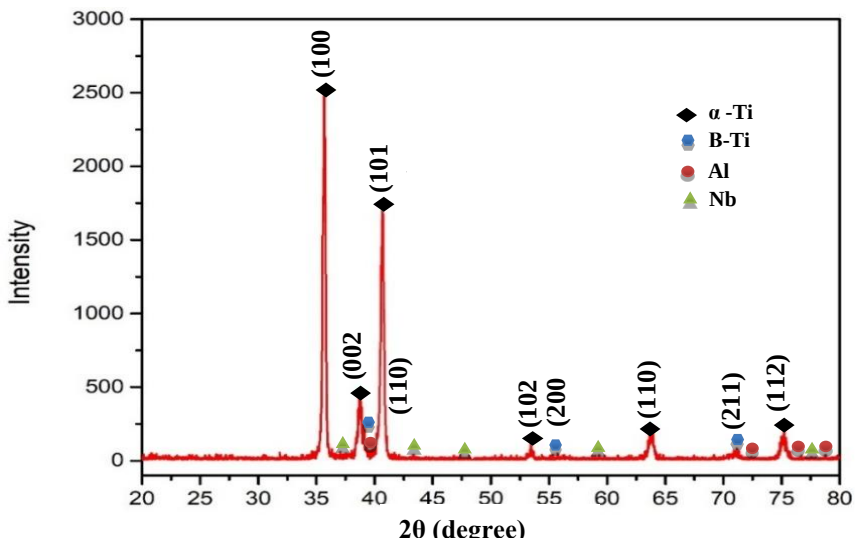

Figure 11: XRD analysis for the Ti-6Al-7Nb alloy as received.

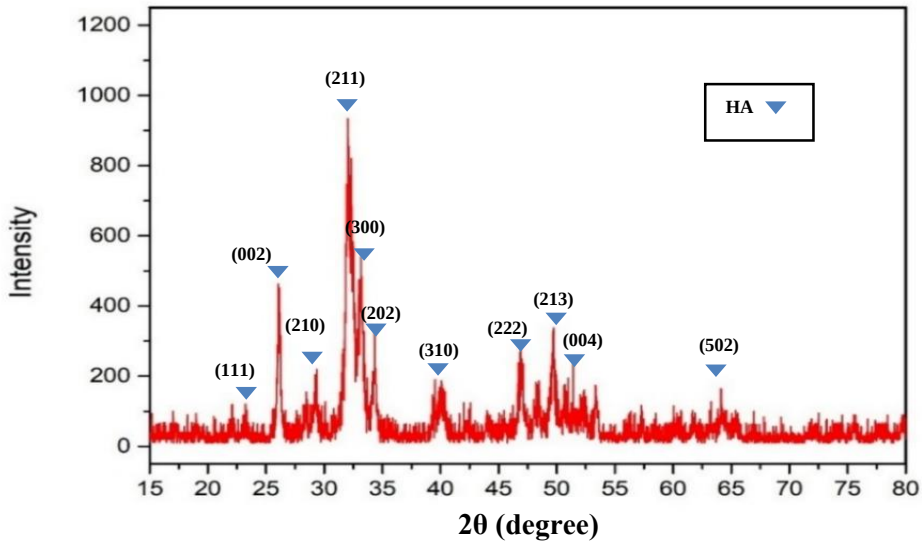

Figure 12: XRD analysis for HA Nano particles.

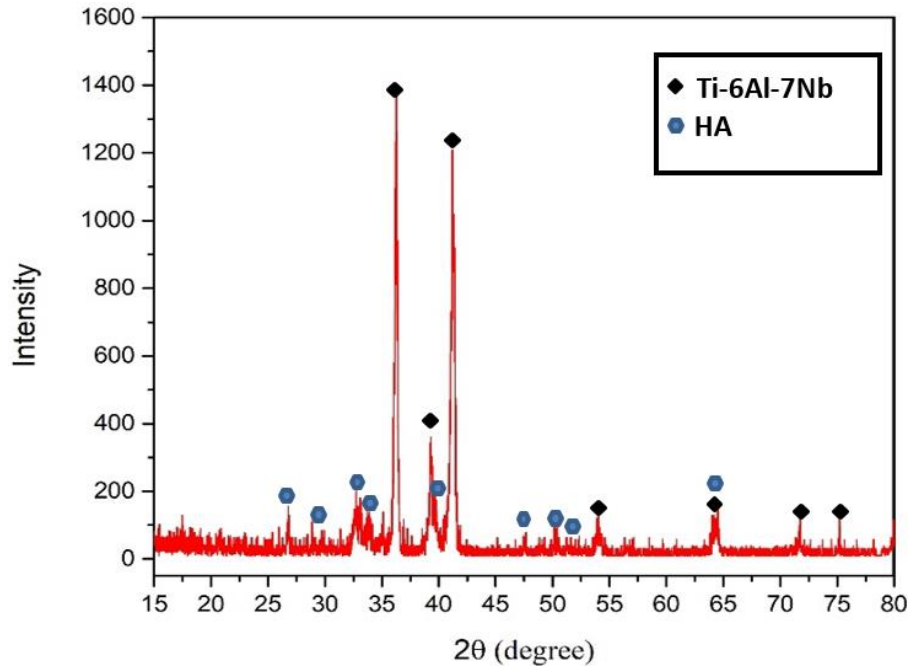

Figure 13: XRD pattern of the composite HA/CS deposit.

5.6. Biocorrosion results

Corrosion current density (i_{corr}) and corrosion potential (E_{corr}) are calculated using the Tafel curve graph by the intersection of the extrapolation of the anode and cathode parts of the polarization curve [29, 30].OCP trends correlated more closely with actual corrosion rates, reflecting passive film stability. Figure 14 presents the potentiodynamic polarization curves obtained for the uncoated Ti_6Al_7Nb and three coated samples 3, 5, and 9 based on the current type in SBF at 37 °C. Table 12 summarizes the corrosion parameters, including open-circuit potential (OCP), current density (i_{corr}), and corrosion potential (E_{corr}). The OCP of all HA/CS-coated Ti_6Al_7Nb shifted significantly in the noble direction, showing higher thermodynamic stability [36]. According to the results, samples with HA/CS coating exhibit a lower corrosion rate (higher corrosion resistance) as measured by corrosion current density compared to the uncoated Ti alloy. The uncoated alloy exhibited the highest corrosion current density value equal to 1.089×10^{-6} A/cm² and corrosion rate 9.662×10^{-3} mm/year, accompanied by a highly negative OCP (−0.552 V), indicating poor corrosion resistance. Sample3 demonstrated the best performance,

with the lowest icorr 2.515×10^{-7} A/cm² and corrosion rate 2.23×10^{-3} mm/year, as well as the most positive OCP (−0.141 V), suggesting a stable passive film despite its highly negative E_{corr} (−0.542V). However, E_{corr} does not always match the actual corrosion rate; sample 3 has the lowest corrosion rate despite being the most negative in E_{corr}, implying strong passivation. Sample 5 showed moderate corrosion resistance with a corrosion rate of 7.948×10^{-3} mm/year and a negative OCP (−0.546V), likely due to limited passivation or localized corrosion. Sample 9 performed well, with a low icorr 2.662×10^{-7} A/cm², a low corrosion rate 2.360×10^{-3} mm/year, and a relatively noble OCP (-0.233 V). Overall, OCP trends correlated more closely with actual corrosion rates than E_{corr}, highlighting the role of passive film stability in controlling corrosion kinetics. HA/CS coating layer formed a protective layer separating the metallic substrate from the corrosive environment [3]. Improvement of corrosion resistance of the metallic substrate after application of the HA/CS coating was observed in other studies [36]. Figure 15 illustrates the topography of samples 3, 5, and 9 after corrosion in SBF at 37 °C. The corrosionresistance of metal implants is crucial because it can affect biocompatibility and mechanical integrity [37]. Coated samples had smoother surfaces with fewer pits compared to the heavily corroded uncoated alloy. In environments that are neutral, alkaline, and just mildly acidic, titanium is stable; below pH ~ 5, it begins to dissolve. Furthermore, inflammation in the human body causes a localized decrease in pH in the tissues around implants [38, 39]. Metallos is and implant rejection may result from corrosion products penetrating the peri-implant tissues under such circumstances [3, 40].

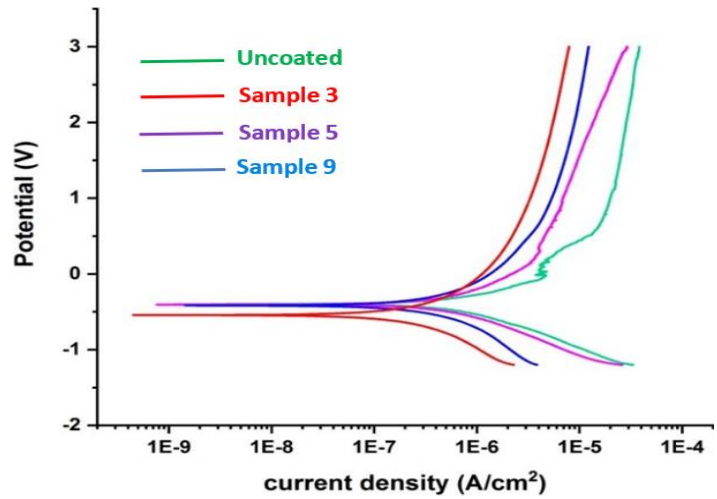

Figure 14: Polarization curves of the coated and uncoated Ti alloy.

Table 12: Open circuit potential, corrosion potential, and current density of the uncoated Ti alloy substrate and coated sample.

ITEM	$E_{corr.}$ (V (SCE))	$I_{corr.}$ (A)	$I_{corr.}$ (A/cm²)	Corr. Rate mm/y	βc	βa	OCP (V)
Uncoated	-0.401	4.195×10^{-7}	1.089×10^{-6}	9.662×10^{-3}	0.214	0.199	-0.552
Sample 3	-0.542	9.683×10^{-8}	2.515×10^{-7}	2.23×10^{-3}	0.205	0.200	-0.141
Sample 5	-0.412	3.451×10^{-7}	8.963×10^{-7}	7.948×10^{-3}	0.231	0.213	-0.546
Sample 9	-0.424	1.025×10^{-7}	2.662×10^{-7}	2.360×10^{-3}	0.212	0.206	-0.233

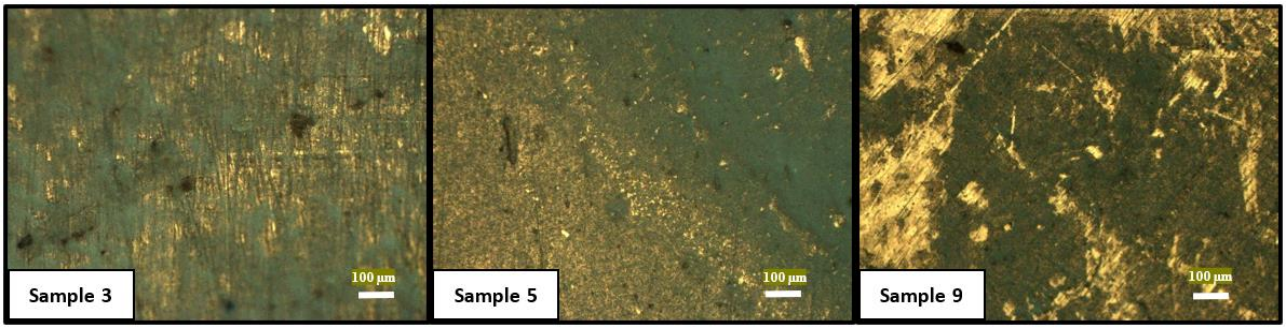

Figure 15: Topography of the samples 3, 5, and 9 after corrosion in SBF at 37 °C.

6. Conclusions

The following conclusions are drawn from the results of the experimental work of this study:

1. The optimal conditions for HA/CS coating on Ti-6Al-7Nb using EPD, considering coating thickness and adhesion between the HA/CS layer and the Ti-6Al-7Nb substrate, were found to be below 70 volts, pulse direct current, 6 minutes of deposition time, and 800 grit grinding degree.

2. The coating significantly enhanced adhesion, uniformity, and corrosion resistance, making Ti-6Al-7Nb with HA/CS coating more reliable for biomedical implants.

3. The X-ray diffraction pattern of the optimal sample indicates that HA/CS is effectively deposited on the Ti-6Al-7Nb alloy substrate through EPD, due to the presence of HA phases. The most intense peak is observed at $2\theta = 32.4°$, corresponding to the (211) plane of HA.

4. The stability of the HA/CS solution for coating deposition was verified by the Zeta potential test, which showed a value of 23 mV.

5. Applying HA/CS coating on Ti alloy via EPD reduced the corrosion rate of the Ti alloy by approximately 23.08 %, thereby improving its corrosion resistance.It shifted open-circuit potential toward nobler values and reduced corrosion rate from 9.662×10^{-3} mm/year (uncoated) to 2.23×10^{-3} mm/year (coated, PDC). PDC enables strong, uniform, corrosion-resistant HA/CS coatings, making it a superior current type for implant surface modification.

6. Based on a statistical analysis (ANOVA) of thicknesses and adhesion of the HA/CS coating layer, the main factors affecting the deposition of the HA/CS layer by EPD technique wereCoating thickness was most influenced by applied voltage (70.3%), while adhesion was dominated by deposition time (80.1%).

7. References

1. Eraković S, Janković A, Veljović D, Palcevskis E, Mitrić M, Stevanović T, et al. Corrosion stability and bioactivity in simulated body fluid of silver/hydroxylapatite and silver/hydroxyapatite/lignin coatings on titanium obtained by electrophoretic deposition. J Phy Chem B. 2013; 117(6):1633-43. https://doi/10.1021/jp305252a.
2. Hameed HA, Hasan HA, Luddin N, Husein A, Ariffin A, Alam MK. Osteoblastic cell responses of copper nanoparticle coatings on Ti-6Al-7Nb alloy using electrophoretic deposition method. Feitosa V, editor. Biomed Res Int. 2022 Jan 19; 2022(1):1. https://doi/10.1155/2022/3675703.
3. Pawłowski Ł, Bartmański M, Strugała G, Mielewczyk-Gryń A, Jażdżewska M, Zieliński A. Electrophoretic deposition and characterization of chitosan/eudragit E 100 coatings on titanium substrate. Coatings. 2020; 10(7):607. https://doi/10.3390/coatings10070607.
4. Moskalewicz T, Seuss S, Boccaccini AR. Microstructure and properties of composite polyether-etherketone/ Bioglass® coatings deposited on Ti-6Al-7Nb alloy for medical applications. Appl Surf Sci. 2013; 273: 62-7. http://dx.doi.org/10.1016/j.apsusc.2013.01.174.
5. Hussein M, Mustafa A, Abdulkareem M. Using taguchi design to compare the corrosion behavior of commercial pure Ti alloys coated by dip and electrophoretic deposition with YSZ. Eng Technol J. 2023; 41(12):1588-603. https://doi/10.56294/sctconf2024847.
6. Moskalewicz T, Kot M, Seuss S, Kędzierska A, Czyrska-Filemonowicz A, Boccaccini AR. Electrophoretic deposition and characterization of HA/chitosan nanocomposite coatings on Ti6Al7Nb alloy. Metal Mater Internat. 2015; 21(1):96-103. https://doi/10.1007/s12540-015-1011-y.

7. Hezil N, Aissani L, Fellah M, Abdul Samad M, Obrosov A, Timofei C, et al. Structural, and tribological properties of nanostructured α + β type titanium alloys for total hip. J Mater Res Technol. 2022; 19:3568-78. https://doi/10.1016/j.jmrt.2022. 06. 042.
8. Cristiano C. Gomes, Leonardo M. Moreira, Vanessa J.S.V. Santos, Alfeu S. Ramos, Juliana P. Lyon CPS and FVS. Assessment of the genetic risks of a metallic alloy used in medical implants. Genet Mol Biol. 2011; 34(1):116-21. https://doi/10.1590/S1415-4757201000 5000118.
9. Baltatu MS, Sandu AV, Nabialek M, Vizureanu P, Ciobanu G. Biomimetic deposition of hydroxyapatite layer on titanium alloys. Micromachines. 2021; 12(12):1-12. https://doi/10.3390/mi12121447.
10. Hanawa T. Metal ion release from metal implants. Mater Sci Eng C. 2004; 24(6-8):745-52. https://doi/ 10.1016/j.msec.2004.08.018.
11. Chlebus E, Kuźnicka B, Kurzynowski T, Dybała B. Microstructure and mechanical behaviour of Ti-6Al-7Nb alloy produced by selective laser melting. Mater Charact. 2011; 62(5):488–95. https://doi/10.1016/j. matchar.2011.03.006.
12. Aydın İ, Bahçepınar Aİ, Kırman M, Çipiloğlu MA. Coating on Ti_6Al_7Nb alloy using an electrophoretic deposition method and surface properties examination of the resulting coatings. Coatings. 2019; 9(6):402. https://doi/10.3390/coatings9060402.
13. Liu X, Poon RWY, Kwok SCH, Chu PK, Ding C. Plasma surface modification of titanium for hard tissue replacements. Surf Coat Technol. 2004; 186(1-2):227-33. https://doi/10.1016/j.surfcoat.2004.02.045.
14. Mistry S, Kundu D, Datta S, Basu D. Comparison of bioactive glass coated and hydroxyapatite coated titanium dental implants in the human jaw bone. Aust Dent J. 2011; 56(1):68-75. https://doi/10.1111/j.1834-7819.2010.01305.
15. Hsu HC, Wu SC, Lin CY, Ho WF. Characterization of hydroxyapatite/chitosan composite coating obtained from crab shells on low-modulus Ti–25Nb–8Sn alloy through hydrothermal treatment. Coatings. 2023; 13(2). https://doi/10.1007/s42242-021-00170-3
16. Khalid S. Almulhim , Mariam Raza Syed , Norah Alqahtani , Marwah Alamoudi MK, Khan SZA. Bioactive inorganic materials for dental applications: a narrative review. Materials; 2022; 15(19): 6864. https://doi.org/10.3390/ma15196864.
17. Kadhim I, Abdul Ameer Z, Alzubaidi A. Synthesis and characterization of chitosan- polyvinyl alcohol blend modified by genipin and nanohydroxyapatite for bone tissue engineering. Eng Technol J. 2019; 37(11A):470-4. https://doi/10.30684/etj.37.11a.4.
18. Mohan L, Durgalakshmi D, Geetha M, Sankara Narayanan TSN, Asokamani R. Electrophoretic deposition of nanocomposite ($HAp+TiO_2$) on titanium alloy for biomedical applications. Ceram Int. 2012;38 (4):3435-43.http://dx.doi.org/10.1016/j.ceramint.2011. 12.056.
19. AL-Shahrabalee S, Jaber H. The impacts of calcium ions substitution in hydroxyapatite with neodymium and zinc on biological properties and osteosarcoma cells. Eng Technol J. 2022; 40(12):1-9. https://doi/ 10.30684/etj.2022.133915.1217.
20. Ahmed I, Jaber H, Salih S. Electrophoretic deposition used to prepare and analyze the microstructure of chitosan/hydroxyapatite nano-composites. Eng Technol J. 2021; 39(11):1693-704 .
21. Moskalewicz T, Kot M, Seuss S, Kędzierska A, Czyrska-Filemonowicz A, Boccaccini AR. Electrophoretic deposition and characterization of HA/ chitosan nanocomposite coatings on Ti_6Al_7Nb alloy. Metal Mater Internat. 2015;21(1):96-103. https://doi/ 10.1007/s12540-015-1011-y.
22. Besra L, Liu M. A review on fundamentals and applications of electrophoretic deposition (EPD).2007; 52:1-61. https://doi/10.1016/j. pmatsci. 2006.07.001
23. Boccaccini AR, Keim S, Ma R, Li Y, Zhitomirsky I. Electrophoretic deposition of biomaterials. J R Soc Interface. 2010;7(5):581. https://doi/10.1098/rsif.2010. 0156.focus.
24. Gaafar MS, Yakout SM, Barakat YF, Sharmoukh W. Electrophoretic deposition of hydroxyapatite/chitosan nanocomposites: the effect of dispersing agents on the coating properties. RSC Adv. 2022; 12(42):27564-81. http://dx.doi.org/10.1039/D2RA03622C.
25. Stevanović M, Djošić M, Janković A, Kojić V, Stojanović J, Grujić S, et al. The chitosan-based bioactive composite coating on titanium. J Mater Res Technol. 2021;15:4461-74. https://doi/10.1016/j.jmrt. 2021.10.072.
26. Pishbin F, Simchi A, Ryan MP, Boccaccini AR. Electrophoretic deposition of chitosan/45S5 Bioglass®composite coatings for orthopaedic applications. Surf Coat Technol. 2011; 205(23-24):5260-8. http://dx.doi.org/10.1016/j.surfcoat.2011.05.026.
27. Pang X, Zhitomirsky I. Electrodeposition of composite hydroxyapatite-chitosan films. Mater Chem Phys. 2005;94(2-3):245-51. http://doi/10.1016/j.mat chemphys. 2005.04.040.
28. Kadhim MJ, Abdulateef NE, Abdulkareem MH. Evaluation of surface roughness of 316L stainless steel substrate on nanohydroxyapatite by electrophoretic deposition. Al-Nahrain J Eng Sci. 2018; 21(1):28. https://doi.org/10.29194/NJES21010028 .
29. Vafa E, Bazargan-Lari R, Bahrololoom ME. Electrophoretic deposition of polyvinyl alcohol/ natural chitosan/bioactive glass composite coatings on 316L stainless steel for biomedical application. Prog Org Coat. 2021;151:106059. https://doi/10.1016/j. porgcoat.2020.106059.
30. Zhang XL, Jiang ZhH, Yao ZhP, Song Y, Wu ZhD. Effects of scan rate on the potentiodynamic polarization curve obtained to determine the Tafel slopes and corrosion current density. Corros Sci. 2009; 51(3):581-7. https://doi/10.1016/j.corsci.2008.12.005.
31. Stępień M, Handzlik P, Fitzner K. Electrochemical synthesis of oxide nanotubes on Ti6Al7Nb alloy and

their interaction with the simulated body fluid. J Solid State Electrochem. 2016;20(10):2651-61. http://doi/10.1007/s10008-016-3258-8.

32. Ajee S, Alzubaydi T, Swadi A. Influence of heat treatment conditions on microstructure of Ti-6Al-7Nb alloy as used surgical implant materials. Eng Technol J. 2007; 25(3):431-42. http://doi/10.30684/etj.25.3.15.
33. Moskalewicz T, Warcaba M, Łukaszczyk A, Kot M, Kopia A, Hadzhieva Z, et al. Electrophoretic deposition, microstructure and properties of multicomponent sodium alginate-based coatings incorporated with graphite oxide and hydroxyapatite on titanium biomaterial substrates. Appl Surf Sci. 2022; 575: 151688. https://doi/10.1016/j.apsusc. 2021.151688.
34. Meng X, Kwon TY, Kim KH. Hydroxyapatite coating by electrophoretic deposition at dynamic voltage. Dent Mater J. 2008; 27(5):666-71. https://doi/10.4012/dmj.27.666 .
35. Shahabi S, Najafi F, Majdabadi A, Hooshmand T, Haghbin Nazarpak M, Karimi B, et al. Effect of gamma irradiation on structural and biological properties of a PLGA-PEG-hydroxyapatite composite. Sci World J. 2014; 2014. http://dx.doi.org/10.1155/2014/420616.
36. Kwok CT, Wong PK, Cheng FT, Man HC. Characterization and corrosion behavior of hydroxyl-apatite coatings on Ti_6Al_4V fabricated by electrophoretic deposition. Appl Surf Sci. 2009; 255(13-14):6736-44. https://doi/10.1002/jbm.b.35342.
37. Mareci D, Ungareanu G, Aelenei DM, Mirza Rosca JC. Electrochemical characteristics of titanium based biomaterials in artificial saliva. Mater Corr. 2007; 58(11):848-56. https://doi/ 10.1002/maco.200704065.
38. Chen Q, Thouas GA. Metallic implant biomaterials. Materials Science and Engineering: R: Reports. 2015; 87:1-57. http//dx.doi.org/10.1016/j.mser.2014.10.001
39. Surmeneva MA, Sharonova AA, Chernousova S, Prymak O, Loza K, Tkachev MS, et al. Incorporation of silver nanoparticles into magnetron-sputtered calcium phosphate layers on titanium as an antibacterial coating. Colloids Surf B Biointerfaces. 2017;156:104-13. http://dx.doi.org/10.1016/j.colsurfb.2017.05.016.
40. Demczuk A, Swieczko-Zurek B, Ossowska A. Corrosion resistance examinations of Ti_6Al_4V alloy with the use of potentiodynamic method in Ringer's and artificial saliva solutions. Adv Mater Sci. 2012; 11(4). https://doi/10.2478/v10077-011-0021-9.

How to cite this article:
Muhi Abdulsahib Y, Mustafa AM, Abdulkareem MH. Optimizing Electrophoretic Deposition Parameters and Corrosion Resistance of Nano-Hydroxyapatite/Chitosan Coatings on Ti-6Al-7Nb Alloy Under Various Current Types. Prog Color Colorants Coat. 2026;19(3):297-315. https://doi.org/10.30509/pccc.2025.167666.1451.